Loop opening and closing dynamics in enzymes: activated or friction-limited? The case of protein tyrosine phosphatases

Kirill Zinovjev,[a] Paul Guénon,[a,b] Carlos A. Ramos-Guzmán,[a] J. Javier Ruiz-Pernía,[a] Damien Laage,[b] Iñaki Tuñón[a,b]*

[a] Departamento de Química Física, Universidad de Valencia, 46100 Burjasot (Spain)
[b] PASTEUR, Département de Chimie, École Normale Supérieure, PSL University, Sorbonne University, CNRS, 75005 Paris (France)

*To whom correspondence should be addressed

Abstract

Protein loop dynamics have recently been recognized as central to enzymatic activity, specificity and stability. However, the factors controlling loop opening and closing kinetics have remained elusive. Here, we combine molecular dynamics simulations with string-method determination of complex reaction coordinates to elucidate the molecular mechanism and rate-limiting step for WPD-loop dynamics in the PTP1B enzyme. While protein conformational dynamics is often represented as diffusive motion hindered by solvent viscosity and internal friction, we demonstrate that loop opening and closing is strongly activated. It is governed by torsional rearrangement around a single loop peptide group and by significant friction caused by backbone adjustments, which can dynamically trap the loop. Considering both torsional barrier and time-dependent friction, our calculated rate constants exhibit excellent agreement with experimental measurements. Furthermore, we show the general applicability of our results to other enzymatic loops, thereby offering new prospects for loop engineering potentially leading to enhanced designs.

Enzymes are complex and flexible structures that can adopt different conformations necessary for their function.[1,2] Conformational changes occur during the enzymatic catalytic cycle, and are often required to accommodate the substrate in the active site, position the catalytic residues correctly for the chemical transformation, and release the reaction product into the bulk. In some cases, these conformational transitions are the slowest step in the catalytic cycle, limiting the enzymatic turnover. Therefore, the mechanism and factors governing the dynamics of enzymatic conformational changes have attracted considerable attention in recent years.[3–7]

One of the most ubiquitous conformational changes observed during the catalytic cycles of enzymes is the closing and opening motions of loops that cover active sites. Loop motion is essential for catalysis in many natural enzymes, such as Dihydrofolate Reductase,[8] Triosephosphate Isomerase[9] or Oritidine 5'-Monophosphate Decarboxylase,[10] to name a few well-known examples. Loop closing over active sites ensures substrate sequestration from the solvent[11] and improves active site preorganization, favoring its desolvation.[12] Experimentally, the structures of the open and closed conformations are accessible via x-ray crystallography[13], while the loop opening and closing kinetics can be measured by NMR relaxation.[14,15] Loop motions are found to occur on a broad range of timescales, typically from picoseconds to milliseconds,[16] and in some cases are the rate-limiting step during the catalytic cycle. There is now growing evidence highlighting the tremendous importance of flexible loop dynamics not only for the regulation of enzymatic activity[17] but also for selectivity and thermal stability,[17,18] and controlling the properties of flexible loops is a promising and attractive avenue to obtain enzymes with tailored features.[17]

However, this requires determining the microscopic factors governing the equilibrium between open/closed forms of enzymatic loops and the kinetics of these interstate conversions, and the latter have so far remained elusive. This is largely due to the complexity of large collective displacements occurring during the loop motions and the delicate balance between protein-protein, protein-solvent, and protein-ligand interactions that are involved. Some insights on the underlying factors controlling protein conformational dynamics can be gained from experimental and numerical studies of protein folding. It was suggested that structural dynamics can be described as a diffusive motion on a rough energy landscape with friction caused both by the solvent viscosity and by intrachain protein interactions.[19–22] However, the large activation energy for loop dynamics measured by temperature-jump experiments[23,24] suggests that this diffusive picture is not adequate for loop opening and closing dynamics and that the process is instead activated. Understanding protein loop dynamics thus requires identifying the molecular rearrangements responsible for this barrier.

The paradigm flexible loop protein that we have selected to investigate this issue is human Protein Tyrosine Phosphatase 1B (PTP1B). It is part of the Protein Tyrosine Phosphatases (PTPs) superfamily of enzymes whose activity is regulated by conformational loop motions.[25] PTP1B is involved in the regulation of insulin and leptin signaling and the signaling of epidermal growth factor.[26] It catalyzes the dephosphorylation of one of the tyrosine residues of its protein substrates in a two-step process involving the cleavage of the tyrosine phosphate monoester, followed by the hydrolysis of the phosphoenzyme intermediate. In the first step, the thiol group of a conserved cysteine (Cys215) acts as a nucleophile, breaking the phosphate bond to a tyrosine residue of the substrate and forming a thiophosphate enzyme intermediate. In the second step, this intermediate is hydrolyzed thanks to the nucleophilic attack performed by a water molecule.[6] Both steps are assisted by an aspartic residue (Asp181) that acts as a general acid/base and lies on a loop known as the WPD-loop, named for the three residues placed in the N-terminal side and conserved in the superfamily, Trp179-Pro180-Asp181 in PTP1B. The WPD-loop is a flexible Ω-loop consisting of a dozen residues (117-188), including the catalytic Asp181. Although this loop can exist in both open and closed conformations (see Figure 1), only the closed-loop form allows catalysis:[27] the loop must be closed to bring the catalytic Asp181 into proximity with the active site. Both open and closed forms have been observed in the apo and holo forms of the protein.[25,28,29] In fact, the substrate can bind to both forms.[27] As seen in **Figure 1**, Asp181 forms a salt bridge with Arg112 in the open state, while in the closed state, the side chain of Asp181 is rotated to establish a new salt bridge with Arg221, a residue of the active site that participates in substrate recognition.
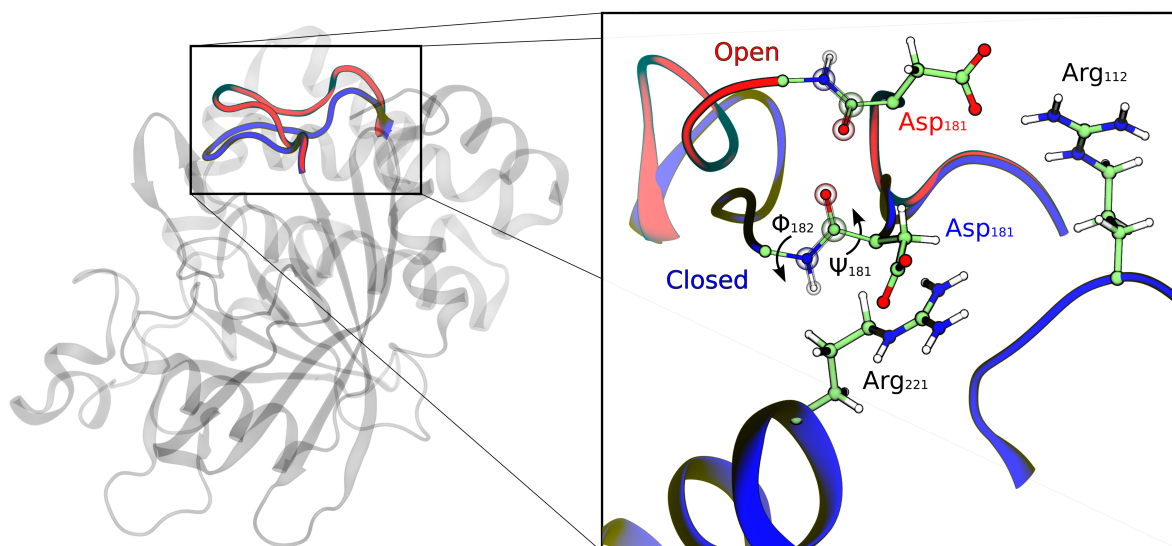

Figure 1. Open and closed states of the WPD-loop in PTP1B. Superposition of the open (red) and closed (blue) loop conformations of PTP1B from PDB structure 6B90. On the right a closer view of the loop highlighting the

positions of residues Phe182, Asp181 and the salt-bridges formed by this latter residue in the open (red) and closed (blue) states with Arg112 and Arg221 respectively. The dihedral angles Φ_{182} and Ψ_{181} controlling the rotation of the peptide bond between residues 181 and 182 are also shown.

The loop opening and closing rate constants have been determined experimentally using NMR techniques. In the apo form of PTP1B, the values obtained for k_{closed} and k_{open} are 22 and 890 s^{-1} respectively, resulting in an equilibrium constant of 40 in favor of the open form.[25] A comparative study between PTP1B and the *Yernisia* PTP (YopH) found that the rates of loop motions mirror the catalytic rate constants in these two enzymes, the rate of loop motions in YopH being about 50 times larger than for PTP1B.[25] However, the barriers found for the chemical steps show only modest differences, suggesting that loop motions contribute to the observed differences in the catalytic rate constants between these two PTPs.[6] Kamerlin, Hengge and coworkers built a series of chimeric enzymes with varied compositions of the WPD-loop, demonstrating that point mutations along the loop can alter the equilibrium between the open and closed states, changing the hydrogen bonding network established by the loop,[27] and affecting the enzymatic activity.[30] In some cases, the increased mobility of chimeric enzymes can result in the exploration of unproductive conformations and consequently in a reduced catalytic rate constant.[31] These results thus stress the key role played by loop dynamics in PTP1B catalytic activity.

While these previous studies have already highlighted important factors contributing to the PTP WPD-loop conformational equilibrium,[6,27,30] a detailed description of the mechanism governing the conformational change of enzymatic loops is still lacking. In this paper, our goal is thus to characterize this mechanism and its rate-limiting step, identify the molecular origin of the large activation energy measured in temperature-jump experiments, and establish the roles of solvent-induced and internal frictions, which had been shown to be important for protein folding dynamics.[21] We combine all-atom molecular dynamics (MD) simulations with a string-method approach to determine the complex reaction coordinate for the open/closed transition and critically, to identify the transition state (TS). Our simulations show that WPD-loop opening in PTP1B results from two successive processes: an activated and localized conformational change in the loop backbone and diffusive loop motions. The key rate-limiting conformational change is the torsion of a single peptide group involving the Asp181 and Phe182 residues. Our analysis of the friction on the reaction coordinate relies on the Grote-Hynes theory to describe the different response timescales in the system and reveals that the relevant friction exclusively arises from the other backbone torsions which need to rearrange when the key dihedral angles switch. This strong friction leads to a dynamical caging effect which considerably slows the barrier crossing. Finally, we show that our novel picture highlighting the importance of single peptide group torsion for loop opening and closing kinetics applies to other PTPs and other

enzymatic systems, thus providing new routes for engineering flexible loop dynamics in proteins.

Results and Discussion

MD simulations of the open/closed state and identification of order parameters.
We ran 10 independent 100 ns long MD simulations for both open and closed states of the PTP1B apo form to analyze the order parameters that distinguish the two states. We monitored all the ψ and ϕ torsion angles of the WPD-loop backbone as well as two distances that correspond to the salt-bridges formed in the open (Asp181Cγ-Arg112Cζ) and closed (Asp181Cγ-Arg221Cζ) states, see **Figure 1**. The values of these distances in the X-Ray open/closed conformations are 4.3/11.5 and 7.8/4.0, respectively.[28]

Figure 2 displays the probability distributions of the distances and torsion angles for simulations in the closed and open states. The analysis of the distances reveals that large transient displacements of the loop are possible, especially for the open state, and that the probability distributions of these distances for the two states overlap. Therefore, it is not possible to distinguish between these two conformational states using only these distances or a function of them (see **Figure S1**). In contrast, two torsional angles ψ_{181} and ϕ_{182} clearly differentiate between both states because their distributions are clearly separated, as shown in **Figures 2** and **S1**. The difference between the two conformational states in terms of these torsions can be explained by the fact that the WPD-loop contains a β-turn defined by four residues, Pro180-Asp181-Phe182-Gly183. When the loop is closed, this β-turn adopts a standard type II conformation,[32] stabilized by a hydrogen bond between the carbonyl group of Pro180 and the NH group of Gly183 (the N-O distance is 2.68 Å in the X-ray structure of the closed form, see **Figure S2**). In the open form, the peptide group between Asp181-Phe182 is rotated, as seen in **Figures 2b and 2c**, with the amide and carbonyl groups pointing in opposite directions to those found in the closed state and the Gly183N-Pro180O distance is now substantially larger, 5.22 Å in the X-ray structure.

This analysis reveals that the open-closed transition of the WPD-loop involves two distinct types of motion: (i) the displacement of the loop, which is reflected in the varying distances between Asp181 and the two anchoring arginines, and (ii) the conformational change of the backbone, particularly the peptide bond between residues Asp181-Phe182. **Figures 2** and **S1** illustrate the different nature of these motions, with broad fluctuations observed in terms of distances, while the torsional angles ψ_{181} and ϕ_{182} clearly differentiate between the two states, indicating that changes in these dihedral angles are related to a free energy barrier between the open and closed forms. Before addressing the selection of an

appropriate reaction coordinate to obtain the free energy profile corresponding to the loop conformational change, it is interesting to understand the reasons for the conformational change of the Asp181-Phe182 peptide bond. As mentioned earlier, the loop closes to attain a catalytically active conformation where the Asp181 residue forms a salt-bridge interaction with Arg221. The formation of this interaction necessitates the rotation of the Asp181-Phe182 peptide bond to prevent repulsion between the carbonyl group and the carboxyl oxygen atoms of Asp181. This repulsion is eliminated when the peptide bond is rotated, and the carbonyl group is positioned towards the inner part of the loop, far from the carboxylate group (see **Figure 1**). Thus, based on MD simulations, it has been observed that the open-closed transitions of the WPD-loop involve not only displacement but also a significant conformational rearrangement.
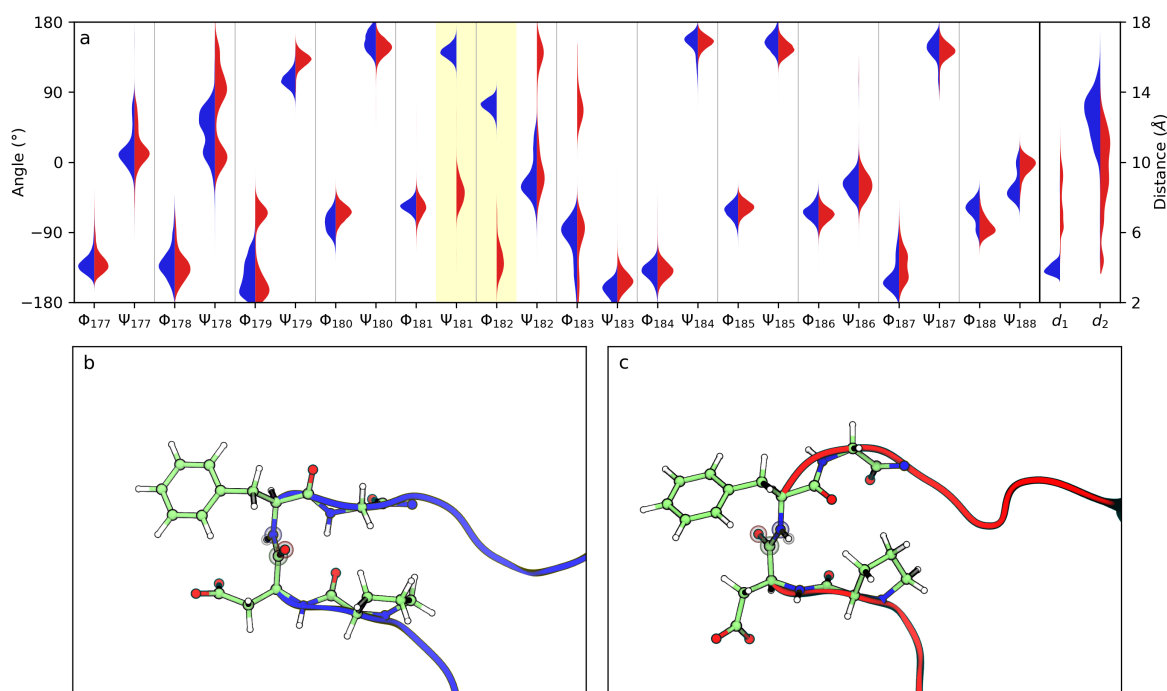

Figure 2. a) Probability distributions of the backbone dihedral angles (ϕ and ψ) corresponding to the WPD-loop obtained from 10x100 ns MD simulations of the open (red) and closed (blue) states along with the distances between the Cγ atom of Asp181 and the Cζ atoms of Arg221 (d_1) and Arg112 (d_2). The two dihedral angles that clearly distinguish the open and closed states are ψ_{181}, ϕ_{182} (highlighted in pale yellow). **b)** Conformation of the Asp181-Phe182 peptide bond in the open conformation. **c)** Conformation of the Asp181-Phe182 peptide bond in the open conformation.

Reaction coordinate and Free Energy Profile for the open/closed transition.

From our previous analysis, it is clear that the ψ_{181} and ϕ_{182} torsional angles are key ingredients of a dividing surface separating the open and closed states and thus of a putative reaction coordinate. Although the salt-bridge distances between Asp181 and

Arg112/Arg221 are not enough to distinguish between the two states, they can still be important to ensure that the transition occurs to the correct structures, particularly in the case of the open state where a wide range of structures exists.[6] Thus, we explored the free energy landscape for the open/closed transition using four collective variables (CVs): ψ_{181}, ϕ_{182}, Asp181Cγ-Arg221Cζ (d$_1$) and Asp181Cγ-Arg112Cζ (d$_2$). We employed the Adaptive String Method (ASM)[33] as explained in the Methodological section. This method determines the Minimum Free Energy Path (MFEP) for the transition and then build a path-CV (denoted as *s*) to obtain a one-dimensional free energy profile using Umbrella Sampling (see Methods).

Figure 3 shows the results of applying the ASM to study the open/closed transition of the WPD-loop in PTP1B. **Figure 3a** shows the Potential of Mean Force (PMF) along the path-CV (*G(s)*). To demonstrate that this method correctly drives the protein from the closed to the open loop conformation, **Figure 3b** shows the RMSD measured for the loop backbone atoms for those structures sampled along the path with respect to the X-Ray structures of the closed and open states. A video of the conformational change along the path is provided as **Video S1**. The *G(s)* profile displays two rugged free energy minima that correspond to the closed (left) and open (right) conformations with a sharp free energy barrier of ~12 kcal·mol^{-1} in between. The minimum corresponding to the closed form has smaller free energy values, the closed conformation being ~1 kcal·mol^{-1} more stable than the open form.

However, the valley corresponding to the open form is significantly wider than that of the closed conformation, reflecting that a larger number of structures are available for the latter state. Obviously, the closed/open equilibrium depends on both factors and the equilibrium constant between these states can be obtained by integrating the free energy profile along the path-CV coordinate as described in the Methods section. The value obtained for the equilibrium constant from our free energy profile is 1.0, indicating that both states are equally probable. In contrast, the experimental value is 40,[25] which translates to a free energy difference of 2.3 kcal·mol^{-1}, the open state being more stable than the closed state. The difference is within the uncertainty of our simulations (see **Figure 3a**). Note that according to our simulations, the free energy of the open state lowers because the corresponding valley along the reaction coordinate is significantly wider and thus that state contains a larger number of possible structures, while the free energy profile (*G(s)*) itself favors the closed state.

Figures 3c and **3d** represent the projection of the path on the antisymmetric combination of distances and torsional angles and the evolution of the individual CVs along the MFEP, respectively. These figures shows that the closed-to-open transition can be decomposed

into three stages, allowing the identification of the transition mechanism and of the rate-limiting step. The first and the third stages essentially correspond to a change in the distances describing the salt bridges between Asp181-Arg112 and Asp181-Arg221. In the transition from the closed to the open state, the Asp181-Arg112 salt bridge must first be broken, and finally, a new salt bridge, Asp181-Arg221, must be formed. These processes take place within each of the two free energy valleys, showing that these salt bridges can be formed or broken with small free energy changes, roughly within 2.0 kcal·mol⁻¹. The disruption of the salt bridges is facilitated by the presence of water molecules that can efficiently shield the charge-charge interaction between Asp181 and the arginine, modulating the energy gain associated to this interaction. This can be seen in the evolution of the number of solvent molecules around the carboxylate group of Asp181, that shows a clear increase in the intermediate stages of the process (see **Figure S3**).
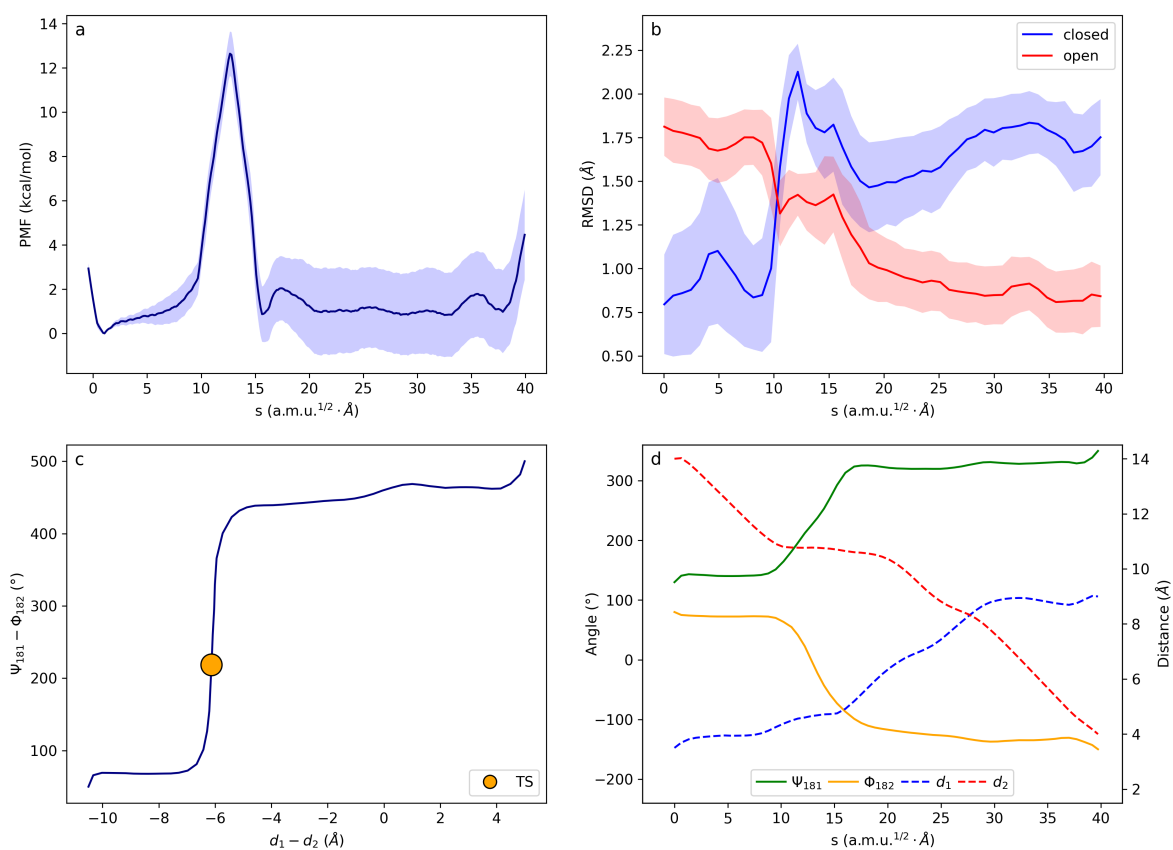

Figure 3. Free energy landscape for the WPD-loop closed to open conformational change in PTP1B. **a)** Free energy profile for the closed (left) to open (right) transition along the *s* path-CV. The shaded region corresponds to the statistical uncertainty; **b)** RMSD for the backbone atoms of the WPD-loop averaged along the MFEP with respect to the X-ray structures (PDB 6B90, that contains both forms) corresponding to the closed (blue) and open (red) states; **c)** Projection of the MFEP along the antisymmetric combinations of the two distances and two dihedral angles used as CVs. The yellow dot point indicates the position of the

Transition State; **d)** Evolution of the individual CVs (distances on the right vertical axis and dihedrals on the left vertical axis) along the MFEP. The CVs used in the ASM calculations are: ψ_{181}, ϕ_{182} torsional angles and the distances Asp181Cγ-Arg221Cζ (d_1) and Asp181Cγ-Arg112 Cζ (d_2).

The second stage of the closed-to-open transition is associated to the change in the ψ_{181} and ϕ_{182} torsional angles. These angles change concertedly, with the first angle increasing and the second angle decreasing. This coordinated motion allows for the complete rotation of the Asp182-Phe182 peptide group (see **Figure 1**). Once the Asp181-Arg221 interaction is broken, the peptide group can be rotated, resulting in the system transitioning to the open state. The open state is then stabilized by the formation of the Asp181-Arg112 salt bridge. This second stage is responsible for the free energy barrier observed in **Figure 3a** and, subsequently, for the rate of the process as discussed below.

According to the picture obtained from our MFEP calculations, the loop opening motion in PTP1B is a combination of two kinds of motions: the loop displacement and the loop backbone conformational rearrangement. The former occurs along a rugged but essentially flat free energy landscape, while the latter is clearly activated. To confirm this picture, we carried out free molecular dynamic simulations for closed state configurations, flipping only the peptide bond between residues 181 and 182, switching the values of ψ_{181}, ϕ_{182} torsional angles from those corresponding to the closed state to those found in the open state (see SI for details). After 1 μs of simulation, 18 of the 20 trajectories resulted in a stable open loop conformation with a significant displacement from the closed position (see **Figure S4a**). Analysis of the loop displacement shows a linear increase of the mean squared Asp181Cα-Gly220Cα distance with time (see **Figure S4b and S4c**), corresponding to a diffusive displacement with a diffusion coefficient of $1.18 \cdot 10^{-2}$ Å$^2 \cdot$ns^{-1}. Considering that, according to the X-ray structures, the Asp181Cα-Gly220Cα distance must increase by 4.4 Å from the closed to the open conformation, a purely diffusive loop motion should be completed in approximately 800 ns. However, the experimental rate constant shows that the PTP1B loop opening/closing process takes place in the millisecond/second time scale,[25] indicating the presence of a free energy barrier separating the closed and open states, in agreement with the proposed PMF. Our free MD simulations demonstrate that flipping a single peptide group, the one between residues 181-182, is the key factor triggering the WPD-loop conformational change in PTP1B, and that the free energy barrier in between the closed and open states is largely associated with the rotation of this particular peptide group. Once this rotation is completed, the loop can diffusively evolve from the closed to the open state. Note that temperature jump studies on different enzymes have demonstrated that loop conformational changes can present a significant activation barrier, in agreement with our picture.[23,24]

Evaluation of the rate constant and the impact of friction in loop motion

According to our previous description, the inverse rate for loop opening motion should be obtained by combining the inverse rates for the loop displacement ($1/k_{dis}$) and for the conformational change associated to the torsion of a single peptide bond ($1/k_{conf}$):

$$\frac{1}{k_{closed/open}} = \frac{1}{k_{dis}} + \frac{1}{k_{conf}} \tag{1}$$

As discussed above, the displacement of the loop is a diffusive motion that takes place in the ns-µs timescale, while the conformational change involves a large associated free energy barrier and takes place in the ms-s timescale. Therefore, we can focus on the latter contribution. Dihedral rotations in general and protein backbone conformational changes in particular, can be modeled as the passage over a one-dimensional free energy barrier subject to the friction exerted by the environment.[19,34,35] This friction results, in principle, from the coupling of solvent and protein degrees of freedom with the reaction coordinate, in this case essentially defined by a combination of the ψ_{181}, ϕ_{182} torsional angles (see TS crossing in **Figure 3c**). We can thus express the rate constant as the product of two terms: one term associated with the free energy barrier that can be derived from Transition State Theory (TST) and a transmission coefficient due to the friction:

$$k_{close/open} = \kappa \cdot k_{close/open}^{TST} \tag{2}$$

The TST rate constant can be obtained from the free energy barrier along the path-collective variable *s* as described in the Methodology section.[36] In the context of protein conformational changes, the transmission coefficient (κ) been usually modelled with Kramers' theory, that considers that the progress along the reaction coordinate can be delayed by frictional effects due to the coupling with the rest of degrees of freedom.[37] In this theory, full friction is exerted during barrier crossing due to an assumed infinitely fast environmental dynamics. However, only part of the environment can respond in the time scale of barrier crossing resulting in significant deviations from the behavior expected by this theory.[38,39] In this study, we used Grote-Hynes (GH) approach based on the generalized Langevin equation to account for frequency-dependent frictional effects on the reaction rate constant (see SI for details).[39] The rate constants corresponding to the opening and closing processes are reported in **Table 1**. The information required for their calculation is provided in **Table S5**. The calculated rate constants closely match the experimental values, with a maximum difference of only one order of magnitude. This can be translated into an error of only 2 kcal·mol^{-1} in the corresponding activation free energies.

Table 1. Experimental and calculated values for the equilibrium and rate constants (in s⁻¹) corresponding to the opening/closing process of the WPD-loop in PTP1B and YoPH.

		$k_{opening}$	$k_{closing}$	K_{eq}
PTP1B	Exp.	890	22	40
	Calc.	470	470	1.0
YoPH	Exp.	42000	1240	34
	Calc.	79000	610	130

The observed agreement between experimental and calculated rate constants supports the theoretical framework chosen to describe the loop opening process. In our approach the rate is determined by a combination of a free energy barrier and a friction term, which enters through the transmission coefficient and slows down the process. Notably, the effect of the friction on the rate constant is not negligible. The value of the transmission coefficient according to GH is κ=0.17 (see **Table S5**), which reduces the rate of the process by almost one order of magnitude with respect to the TST estimation. Although the value of κ is small, Kramers' prediction is significantly smaller (κ_Kr=0.05), indicating that this theory overestimates the effect of friction by ignoring its time-dependence, as previously recognized.[38,39] Importantly, the value predicted by the GH theory agrees with the calculated ratio of reactive trajectories estimated from the free trajectories initiated at the TS depicted in **Figure S5** (13 out of 60 trajectories are reactive, this is evolve from closed to open state, some of them displaying recrossings).

The molecular origin of friction during protein folding processes has been long discussed in the literature. In general, both solvent and protein degrees of freedom contribute to this friction, but the extent of their participation seems to be case-dependent.[19,21,35,40] Our framework provides a strategy for a systematic analysis. The time-dependent friction and its power spectra for the conformational change of the PTP1B WPD-loop are presented in **Figure 4**. The friction exerted by the environment on the reaction coordinate is so high, the friction at t=0 equals $960\ cm^{-1}$, that it surpasses the force produced by the underlying free energy barrier $-\frac{1}{2}\omega_{eq}^2(s-s^{\ddagger})$, where $\omega_{eq} = 409\ cm^{-1}$. This indicates that the motion of the system at the TS enters the so-called polarization caging regime (different friction regimes in GH theory are discussed in the SI).[41] In this regime, the environment can trap the system in the TS region and motion of the coupled degrees of freedom is required to relax the system off the TS. The analysis of the free trajectories started at the TS reveals such a caging regime, where the system remains in the TS region for several ps in some of the trajectories (see **Figure S5**).

To determine which degrees of freedom are coupled to the reaction coordinate we recalculated the friction coming from the forces exerted by the solvent and the protein separately, taking advantage of the pairwise nature of the force field. In this last case we further decomposed the contribution to the friction coming from different inter- and intra-molecular contributions (backbone and sidechain torsions). **Figures 4a** shows different contributions to the total friction including solvent and protein intramolecular contributions (stretching, bending and torsions), which demonstrate that the protein term almost entirely determines the friction acting on the loop conformational change. **Figure 4b** shows the power spectrum of the friction, focusing on the lower frequency region. Slower movements are responsible for the deviation of the transmission coefficient from unity since these motions may lag behind the progress of the system along the reaction coordinate, causing the trajectory to return to the reactants valley or the caging effect mentioned above. An analysis of the friction power spectrum indicates that some stretching/bending contributions appear in the 200-700 cm^{-1} region while torsions mainly appear in the region below 400 cm^{-1} and constitute the only contribution below 200 cm^{-1}. Among these torsions, ϕ and ψ backbone angles make the most significant contribution to the friction, indicating the resistance of the loop backbone to follow the rotation of the Asp181-Phe182 peptide group. **Figure S6** shows a Fourier Transform analysis of the motion of the ϕ and ψ backbone angles coupled to the reaction coordinate at the TS, which shows that the low frequency contributions to the friction are largely dominated by two particular torsions, ψ_{182} (from Phe182) and ϕ_{183} (from Gly183). As discussed below, this indicates that the magnitude of the torsional friction is sequence dependent.
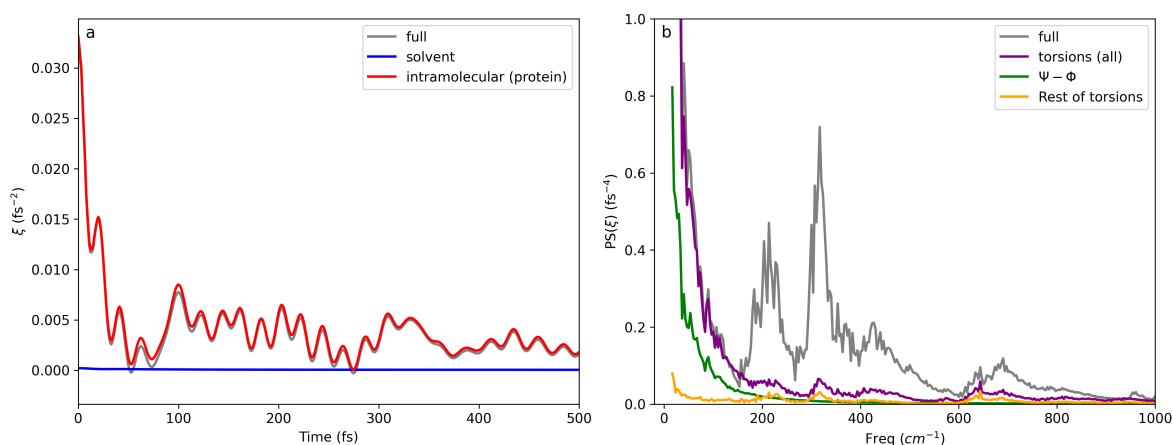

Figure 4. Contributions to the friction acting on the conformational change of the WPD-loop in PTP1B. **a)** Time-dependent friction acting on the reaction coordinate for the closed to open loop transition in PTP1B, calculated at the TS. The total friction is decomposed into contributions from solvent and intramolecular protein forces, which is responsible for almost all the friction; **b)** Power spectra of the total friction and the contribution caused by torsions, separating the contributions of backbone torsions (ϕ and ψ) from the remaining protein torsions.

To our knowledge, this is the first study that has rigorously decomposed the contributions to the friction that occurs during a protein conformational change (within the pairwise approximation of the force field). Our findings reveal that the torsional motions of the loop backbone resist the conformational change. In the context of protein folding, time-resolved fluorescence anisotropy has been used to show that short-range backbone dihedrals cause the friction acting during conformational transitions of intrinsically disordered proteins.[22] Furthermore, simulations of peptide and protein folding processes have shown that internal friction effects can be ascribed to torsional barriers.[19,38] In the case of loop opening/closing motion in PTP1B, we have demonstrated that barrier crossing takes place under strong internal friction due to the accommodation of those torsions that are coupled to the conformational change. This coupling can be efficiently captured as a time-dependent friction acting on a properly chosen reaction coordinate. It must be emphasized that while friction can account for a rate constant reduction roughly by a factor of 10, the barrier height remains the main factor controlling loop kinetics.

Extension to YopH and other systems

The proposed mechanism for the opening/closing conformational change of a loop consists of two types of motions: diffusive displacement and activated torsional rearrangement. The torsional rearrangement occurs around a specific peptide group, such as Asp181-Phe182 in the WPD-loop of PTP1B. The resistance of the rest of the loop to the conformational transition can be considered as a frictional force acting on the reaction coordinate. We believe that this picture can be generalized and extended to other protein loops. Upon inspection of several X-ray structures of enzymes with loops in open and closed conformations, we have observed that the torsional difference between the backbones in the two conformations is primarily due to the rotation of a single peptide group. For example, in the case of *E. coli* Dihydrofolate Reductase,[42] the primary difference between the open and closed forms of loop M20 is the rotation of the Asn18-Ala19 peptide group. In the case of Triosephosphate Isomerase, the open and closed forms of loop 6[43,44] differ in the orientation of the carbonyl and amide groups of the Leu174-Ala175 peptide group. A similar difference is observed for the loop closing the active site in Lactate Dehydrogenase (Arg105-Leu106 peptide group in the rabbit version).[45] Finally, in the case of the Zika virus helicase,[46] the conformational change of motif V involves the rotation of the Met414-Gly415 peptide group.

A particularly interesting system is the YopH, another member of the PTP family that also contains a WPD-loop, like PTP1B. The WPD-loop of YopH has a β-turn but composed in this case by residues Pro355-Asp356-Gln357-Thr358. Another difference between the two

enzymes is that the catalytic aspartate of YopH (Asp356) forms a salt bridge with an arginine (Arg409) only in the closed state, whereas in the open state, Asp356 interacts with Ser289. The main difference in conformation between the loop backbones in the open and closed forms of the YopH loop is the rotation of the peptide group Asp356-Gln357 (see **Figure S2**). Interestingly, the experimental rate constant for loop opening in YopH is about two orders of magnitude larger than that of PTP1B.[25] As explained in the methodological section, we followed a similar computational protocol to that used in PTP1B to estimate the rate and equilibrium constants for the open/closed conformational change of the WPD-loop in YopH. The values obtained for the rate and equilibrium constants for the loop change in YopH (see **Table 1**) are in excellent agreement with the experimental observations.

To understand the similarities and differences between the conformational changes of the WPD-loop in PTP1B and YopH, we analyze the MFEP obtained for the latter in **Figure 5a**. The picture obtained for the loop conformational change in YopH is very similar to that described for PTP1B: the process is a combination of a diffusive displacement of the loop and an activated rotation of the Asp356-Gln357 peptide group (see evolution of distances and torsional angles in **Figure 5b**). However, the free energy barrier in YopH is about 3 kcal·mol^{-1} smaller than in the case of PTP1B, which explains the observed increase in the rate constants. One contribution to the reduced activation free energy for loop opening in YopH with respect to PTP1B is the composition of the β-turn. The residue in the fourth position of this β-turn is bulkier in YopH than in the WPD-loop of PTP1B (Thr358 in YopH versus Gly183 in PTP1B). This results in a weaker hydrogen bond between the carbonyl group of the first residue and the NH group of the fourth residue of the β-turn in the case of YopH, as seen in **Figure S2**. This difference may be the origin of the increased free energy barrier in PTP1B, because this intra-β-turn hydrogen bond must be broken at the TS (see **Figure S7**).
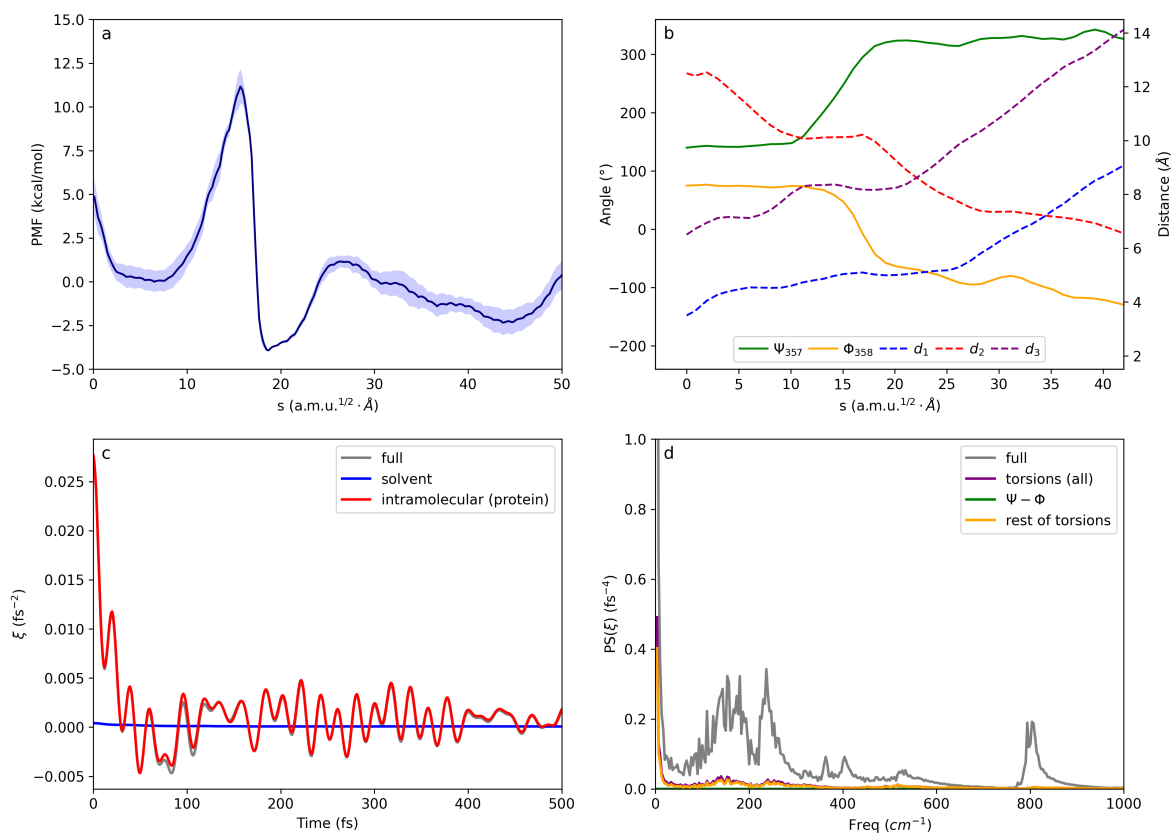
Figure 5. Results for the closed to open conformational change of the WPD-loop in YopH. **a)** Free energy profile for the closed (left) to open (right) transition along the *s* path-CV as obtained from the string method. The shaded region corresponds to the statistical uncertainty; **b)** Evolution of the individual CVs (distances in right vertical axis and dihedrals left vertical axis) along the MFEP. The selected CVs are the torsional angles ψ_{357}, ϕ_{358} and the distances Asp356Cγ-Arg409Cζ (d_1), Asp356Cγ-Ser289 Oγ (d_2) and Asp356Cα-Gly408Cα (d_3). **c)** Time-dependent friction acting on the reaction coordinate for the closed to open loop transition calculated at the TS. The total friction is decomposed in contributions coming from solvent and intramolecular protein contributions, the latter is responsible for most of the friction; **d)** Power spectra of the total friction and the contribution due to torsions, with the contributions of backbone (ϕ and ψ) separated from the rest of the protein torsions.

The time-dependent friction acting on the reaction coordinate for the loop change is presented in **Figure 5c**. The friction is smaller for YopH than in the case of PTP1B, but still corresponds to a caging regime where the initial friction is larger than the equilibrium reaction frequency (see **Table S5**). The transmission coefficient obtained for YopH is larger than for PTP1B: 0.24 versus 0.17, reflecting the smaller value of the friction. This friction in YopH is also dominated by intramolecular contributions to the force field, and the role of intermolecular interactions is negligible. The power spectra (**Figure 5d**) shows that the reduced friction in YopH compared to PTP1B is due to the smaller contribution of backbone torsions in YopH, which dominate the friction at low frequencies below 50 cm^{-1}, while in

PTP1B backbone torsions were predominant already at 200 cm^{-1}. The comparison of the Fourier transforms of the time evolution of the backbone torsions coupled to the reaction coordinate show that the lack of Phe and Gly at positions three and four of the β-turn explains the differences observed in the friction acting on both enzymes These observations suggest that the internal friction arising due to torsional relaxation is controlled by the local sequence composition, in agreement with a recent experimental study on the origin of friction in the folding of intrinsically disordered proteins.[40]

Conclusions

Loop motions are crucial constituents of protein dynamics during the catalytic cycle of many enzymes. Loop opening and closing allow the binding of the substrate in the active site and/or bring different reaction partners together within adequate distances and orientation. Therefore, understanding the mechanisms that govern loop motions is necessary to rationalize enzyme behavior and to engineer better biocatalysts. In this study, we conducted a computational analysis of the opening/closing conformational change of the WPD-loop in two PTP enzymes, PTP1B and YopH. This loop contains one of the key residues for the phosphatase activity of these enzymes, Asp181 or Asp356, and loop closing over the active site is a necessary step for catalysis. Our simulations are based on a path collective variable that depends on a combination of few distances and torsions that define the position of the loop and the conformational changes in the backbone. The rate constants for the loop opening and closing transitions obtained within this picture are in excellent agreement with experimental observations for both the WPD-loop of PTP1B and YoPH. According to our findings, the transition of the loop between the closed and open conformations can be described as a combination of a diffusive displacement of the loop and a torsional rearrangement that requires crossing a significant barrier. This free energy barrier is associated with the torsional rearrangement of the two dihedral angles that govern the rotation of a single peptide group, Asp181-Phe182 or Asp356-Gln357 in PTP1B and YoPH, respectively. The remaining torsions of the loop backbone must adapt to this conformational change, offering a resistance that translates into a strong friction acting during the barrier crossing event. The contribution to the friction due to other degrees of freedom, particularly those of the solvent, is of minor importance here. We have also shown that the friction is correctly incorporated to the rate constant using Grote-Hynes equation, while Kramers' approximation overestimates the effect of this friction by ignoring its frequency-dependence. For the loop conformational transition, the friction is so strong that the barrier crossing is found in the so-called polarization cage regime. In this regime, the motion of the slow environmental degrees of freedom, such as the rest of torsions of the loop backbone, is required for the system to relax off the transition state region. This

observation is also relevant for the treatment of internal friction in the study of protein folding processes, which is mainly due to torsional degrees of freedom.

Engineering of enzymatic loops has attracted an increased attention as a strategy to alter enzymatic function, stability, and specificity. The framework presented here offers an opportunity to rationalize the consequences of mutations on loop kinetics. It reveals how mutations can increase/decrease loop kinetics by decreasing/increasing the torsional barrier associated to the backbone rearrangement. This is mostly a local effect around a particular peptide group that can be understood in terms of changes in protein-loop and/or intra-loop interactions. On the other side, mutations can also contribute to a fine tuning of loop kinetics through a change in the friction, which is a more collective effect involving the rearrangement of the whole loop backbone. This picture can be extended not only to loop motions in other enzymatic systems, but also to lid motions[47] and conformational changes of larger protein motifs, which could involve a few key torsional rearrangements determining the barrier height accompanied by an extensive backbone readaptation entering as a friction into the rate constant. As the importance of protein conformational dynamics is increasingly recognized, identifying the molecular rearrangements that control its kinetics is critical.

Methodology

Preparation of the system.

The simulation PTP1B system was based on the PDB structure 6B90, which contains the enzyme with the studied loop in both states (closed and open). The missing residues were taken from PDB structure 4Y14 after aligning it using PyMOL.[48] The hydrogen atoms and tautomeric states were assigned with pdb4amber from AmberTools20. The protonation states were assigned with Propka 3.0[49] at pH=7.0. The protonated PTP1B structures (with closed and open loop) were described using with ff19SB forcefield.[50] OPC water[51] box and sodium counterions were added with tleap from AmberTools20.[52] The two systems were then minimized, the simulation box size was relaxed by running 100ps of NPT MD followed by 100 ns of NVT MD using pmemd of Amber20.[52] Full details of the equilibration and simulation protocol are given in the SI. Except when indicated, all simulations employed a timestep of 2 fs and the SHAKE algorithm[53] was used to constrain bond lengths. Periodic boundary conditions were applied, long range electrostatic interactions were treated with PME[54] and a non-bonded cutoff distance of 8.0 Å was used for van der Waals interactions. Langevin thermostat was used to control the temperature with a collision frequency of 2.0 ps^{-1}. The same system preparation and relaxation protocol was used for the YopH system. In this case the starting PDB structures for the closed and open states were 1YPT and 2I42, respectively, removing the vanadate ion present in the active site of the latter. Missing C-terminal residues in 1YPT were added from 2I42. See Data availability section for the files containing parameters and relaxed structures of the two enzymes in the two states.

Conventional Molecular Dynamics.

The thermodynamic ensembles of PTP1B and YoPH with the loop in closed and open states were obtained by running 10 x 100 ns NVT simulations in each of the two states, starting from snapshots taken every 5 ns from the last 50ns of the relaxation MD. To probe the response of the loop to the conformational change in the β-turn of PTP1B, 20 replicas starting from different structures with "closed" loop were run with dihedral restraints that force the flip of the peptide bond. Then the restraints were removed, and the replicas were allowed to evolve for 1 µs each. These MD simulations used the same specifications as indicated above.

String simulations

Adaptive string method (ASM)[33] calculations were performed to capture both the local conformational change of the β-turn (controlled by torsional angles) and the loop displacement (controlled by distances). In ASM simulations are carried out over a series of replicas of the system (string nodes) centered at different positions in the space of collective variables (CVs) formed by the set of dihedrals and distances. The string nodes (60 in both

enzymes) evolve towards lower free energy regions while being evenly distributed, which ensures convergence to the MFEP. Half of the nodes were initiated with structures taken from the simulations of the closed state and half from the open state. Hamiltonian replica exchange was attempted between neighboring string nodes every 250 simulation steps. Once the string has converged, a single path-CV, denoted as *s*, is used as a reaction coordinate for subsequent umbrella sampling free energy calculations, accumulating 10-15 ns per node. The initial guesses and the definitions of CVs for both string calculations are provided in the SI together with details about convergence and production times to obtain the free energy profiles.

Calculation of equilibrium and rate constants and the associated free energies

The equilibrium constant between the open and closed forms of the loop were obtained after integration of the PMF along the reaction coordinate (*s*):

$$K_{eq} = \frac{\int_{s>s^\ddagger} C_s^{-1} \cdot e^{-\frac{G(s)}{k_B T}} ds}{\int_{s<s^\ddagger} C_s^{-1} \cdot e^{-\frac{G(s)}{k_B T}} ds} \tag{1}$$

where C_s is a normalization constant with units of the *s* coordinate (1 a.m.u.$^{1/2}$·Å) and $s^\ddagger$ is the position of the TS.

The TST rate constant can be obtained from equilibrium flux across the dividing surface defined by the path-collective variable *s*:[36]

$$k^{TST} = \frac{1}{2} \langle |\dot{s}| \rangle_\ddagger \cdot C_s^{-1} \cdot exp\left[-\frac{\Delta G_s^\ddagger}{k_B T}\right] \tag{4}$$

The preexponential term in eq. (4) contains the normalization constant and the average modulus of the velocity along the reaction coordinate at the TS that was obtained assuming a Maxwell-Boltzmann distribution and the reduced masses of the reaction coordinate at the TS (0.917 and 1.032 for PTP1B and YopH, respectively). The term in the exponential contains the free energy difference between reactants (closed/open states) and the TS:

$$\Delta G_s^\ddagger = G(s^\ddagger) - k_B T \cdot ln \int_s \ C_s^{-1} \cdot e^{-\frac{G(s)}{k_B T}} ds \tag{5}$$

The reaction and activation free energies were then derived from the equilibrium and rate constants, respectively:

$$\Delta G_{eq} = -k_B T \cdot ln K_{eq}$$

$$\Delta G_i^\ddagger = -k_B T \cdot ln \frac{k_i h}{k_B T} = -k_B T \cdot ln \frac{\kappa k_i^{TST} h}{k_B T}$$

where *i* stands for closing/opening processes.

Grote-Hynes Simulations

Using the fluctuation-dissipation theorem, the time-dependent friction acting on the reaction coordinate at the TS can be calculated from the autocorrelation of the forces projected on the reaction coordinate (F_s):

$$\xi(t) = \frac{1}{k_B T} \langle F_s(0) \cdot F_s(t) \rangle_{\ddagger} \tag{6}$$

where we assumed mass-weighted coordinates.

Under the effect of this friction, the reaction frequency (ω_r) for crossing a free energy barrier equal to $-\frac{1}{2}\omega_{eq}^2(s - s^{\ddagger})$ is given by the GH equation:[39]

$$\omega_r^2 - \omega_{eq}^2 + \omega_r \cdot \int_0^t \xi(t) \cdot e^{-\omega_r \cdot t} \cdot dt = 0 \tag{7}$$

The difference with respect to Kramers' theory is due to the fact that the effect of the friction is modulated by the reaction frequency, appearing inside the integral in eq (7). Using GH equation, the transmission coefficient appearing in eq (3) is simply obtained as the ratio between both frequencies:

$$\kappa = \frac{\omega_r}{\omega_{eq}} \tag{8}$$

The friction was obtained as an average over 60 independent TS trajectories, where the initial configurations were selected from string simulations at the top of the PMF. To decompose the different contributions to the friction, the forces were recalculated using the same configurations but zeroing different contributions to the MM force field. Details of Grote-Hynes simulations are provided in the SI.

Data availability

Raw data and notebooks for figures, parameters files and coordinates of relaxed open and closed states of PTP1B and YopH are available at https://github.com/emedio/loop-dynamics.

Conflict of Interest

There are no conflicts to declare.

References

(1)   Villali, J.; Kern, D. Choreographing an Enzyme's Dance. *Curr. Opin. Chem. Biol.* **2010**, *14* (5), 636–643. https://doi.org/10.1016/j.cbpa.2010.08.007.

(2)   Richard, J. P. Protein Flexibility and Stiffness Enable Efficient Enzymatic Catalysis. *J. Am. Chem. Soc.* **2019**, *141* (8), 3320–3331. https://doi.org/10.1021/jacs.8b10836.

(3)   McGeagh, J. D.; Ranaghan, K. E.; Mulholland, A. J. Protein Dynamics and Enzyme Catalysis: Insights from Simulations. *Biochim. Biophys. Acta BBA - Proteins Proteomics* **2011**, *1814* (8), 1077–1092. https://doi.org/10.1016/j.bbapap.2010.12.002.

(4)   Gora, A.; Brezovsky, J.; Damborsky, J. Gates of Enzymes. *Chem. Rev.* **2013**, *113* (8), 5871–5923. https://doi.org/10.1021/cr300384w.

(5)   Kohen, A. Role of Dynamics in Enzyme Catalysis: Substantial versus Semantic Controversies. *Acc. Chem. Res.* **2015**, *48* (2), 466–473. https://doi.org/10.1021/ar500322s.

(6)   Crean, R. M.; Biler, M.; van der Kamp, M. W.; Hengge, A. C.; Kamerlin, S. C. L. Loop Dynamics and Enzyme Catalysis in Protein Tyrosine Phosphatases. *J. Am. Chem. Soc.* **2021**, *143* (10), 3830–3845. https://doi.org/10.1021/jacs.0c11806.

(7)   Romero-Rivera, A.; Corbella, M.; Parracino, A.; Patrick, W. M.; Kamerlin, S. C. L. Complex Loop Dynamics Underpin Activity, Specificity, and Evolvability in the (Bα)$_8$ Barrel Enzymes of Histidine and Tryptophan Biosynthesis. *JACS Au* **2022**, *2* (4), 943–960. https://doi.org/10.1021/jacsau.2c00063.

(8)   Singh, A.; Fenwick, R. B.; Dyson, H. J.; Wright, P. E. Role of Active Site Loop Dynamics in Mediating Ligand Release from *E. Coli* Dihydrofolate Reductase. *Biochemistry* **2021**, *60* (35), 2663–2671. https://doi.org/10.1021/acs.biochem.1c00461.

(9)   Liao, Q.; Kulkarni, Y.; Sengupta, U.; Petrović, D.; Mulholland, A. J.; van der Kamp, M. W.; Strodel, B.; Kamerlin, S. C. L. Loop Motion in Triosephosphate Isomerase Is Not a Simple Open and Shut Case. *J. Am. Chem. Soc.* **2018**, *140* (46), 15889–15903. https://doi.org/10.1021/jacs.8b09378.

(10)   Goryanova, B.; Amyes, T. L.; Richard, J. P. Role of the Carboxylate in Enzyme-Catalyzed Decarboxylation of Orotidine 5'-Monophosphate: Transition State Stabilization Dominates Over Ground State Destabilization. *J. Am. Chem. Soc.* **2019**, *141* (34), 13468–13478. https://doi.org/10.1021/jacs.9b04823.

(11)   Malabanan, M. M.; Amyes, T. L.; Richard, J. P. A Role for Flexible Loops in Enzyme Catalysis. *Curr. Opin. Struct. Biol.* **2010**, *20* (6), 702–710. https://doi.org/10.1016/j.sbi.2010.09.005.

(12)   Richard, J. P.; Amyes, T. L.; Goryanova, B.; Zhai, X. Enzyme Architecture: On the Importance of Being in a Protein Cage. *Curr. Opin. Chem. Biol.* **2014**, *21*, 1–10. https://doi.org/10.1016/j.cbpa.2014.03.001.

(13)   Woldeyes, R. A.; Sivak, D. A.; Fraser, J. S. E Pluribus Unum, No More: From One Crystal, Many Conformations. *Curr. Opin. Struct. Biol.* **2014**, *28*, 56–62. https://doi.org/10.1016/j.sbi.2014.07.005.

(14)   Kleckner, I. R.; Foster, M. P. An Introduction to NMR-Based Approaches for Measuring Protein Dynamics. *Biochim. Biophys. Acta BBA - Proteins Proteomics* **2011**, *1814* (8), 942–968. https://doi.org/10.1016/j.bbapap.2010.10.012.

(15)   Palmer, A. G. I. Enzyme Dynamics from NMR Spectroscopy. *Acc. Chem. Res.* **2015**,

48 (2), 457–465. https://doi.org/10.1021/ar500340a.

(16)   Gu, Y.; Li, D.-W.; Brüschweiler, R. Decoding the Mobility and Time Scales of Protein Loops. *J. Chem. Theory Comput.* **2015**, *11* (3), 1308–1314. https://doi.org/10.1021/ct501085y.

(17)   Corbella, M.; Pinto, G. P.; Kamerlin, S. C. L. Loop Dynamics and the Evolution of Enzyme Activity. *Nat. Rev. Chem.* **2023**, 1–12. https://doi.org/10.1038/s41570-023-00495-w.

(18)   Nestl, B. M.; Hauer, B. Engineering of Flexible Loops in Enzymes. *ACS Catal.* **2014**, *4* (9), 3201–3211. https://doi.org/10.1021/cs500325p.

(19)   de Sancho, D.; Sirur, A.; Best, R. B. Molecular Origins of Internal Friction Effects on Protein-Folding Rates. *Nat. Commun.* **2014**, *5* (1), 4307. https://doi.org/10.1038/ncomms5307.

(20)   Zheng, W.; De Sancho, D.; Hoppe, T.; Best, R. B. Dependence of Internal Friction on Folding Mechanism. *J. Am. Chem. Soc.* **2015**, *137* (9), 3283–3290. https://doi.org/10.1021/ja511609u.

(21)   Chung, H. S.; Piana-Agostinetti, S.; Shaw, D. E.; Eaton, W. A. Structural Origin of Slow Diffusion in Protein Folding. *Science* **2015**, *349* (6255), 1504–1510. https://doi.org/10.1126/science.aab1369.

(22)   Das, D.; Mukhopadhyay, S. Molecular Origin of Internal Friction in Intrinsically Disordered Proteins. *Acc. Chem. Res.* **2022**, *55* (23), 3470–3480. https://doi.org/10.1021/acs.accounts.2c00528.

(23)   Nie, B.; Lodewyks, K.; Deng, H.; Desamero, R. Z. B.; Callender, R. Active-Loop Dynamics within the Michaelis Complex of Lactate Dehydrogenase from *Bacillus Stearothermophilus*. *Biochemistry* **2016**, *55* (27), 3803–3814. https://doi.org/10.1021/acs.biochem.6b00091.

(24)   Thompson, M. C.; Barad, B. A.; Wolff, A. M.; Sun Cho, H.; Schotte, F.; Schwarz, D. M. C.; Anfinrud, P.; Fraser, J. S. Temperature-Jump Solution X-Ray Scattering Reveals Distinct Motions in a Dynamic Enzyme. *Nat. Chem.* **2019**, *11* (11), 1058–1066. https://doi.org/10.1038/s41557-019-0329-3.

(25)   Whittier, S. K.; Hengge, A. C.; Loria, J. P. Conformational Motions Regulate Phosphoryl Transfer in Related Protein Tyrosine Phosphatases. *Science* **2013**, *341* (6148), 899–903. https://doi.org/10.1126/science.1241735.

(26)   Zhang, Z.-Y. Protein Tyrosine Phosphatases: Prospects for Therapeutics. *Curr. Opin. Chem. Biol.* **2001**, *5* (4), 416–423. https://doi.org/10.1016/S1367-5931(00)00223-4.

(27)   Shen, R.; Crean, R. M.; Johnson, S. J.; Kamerlin, S. C. L.; Hengge, A. C. Single Residue on the WPD-Loop Affects the PH Dependency of Catalysis in Protein Tyrosine Phosphatases. *JACS Au* **2021**, *1* (5), 646–659. https://doi.org/10.1021/jacsau.1c00054.

(28)   Keedy, D. A.; Hill, Z. B.; Biel, J. T.; Kang, E.; Rettenmaier, T. J.; Brandão-Neto, J.; Pearce, N. M.; von Delft, F.; Wells, J. A.; Fraser, J. S. An Expanded Allosteric Network in PTP1B by Multitemperature Crystallography, Fragment Screening, and Covalent Tethering. *eLife* **2018**, *7*, e36307. https://doi.org/10.7554/eLife.36307.

(29)   Barford, D.; Flint, A. J.; Tonks, N. K. Crystal Structure of Human Protein Tyrosine Phosphatase 1B. *Science* **1994**, *263* (5152), 1397–1404. https://doi.org/10.1126/science.8128219.

(30)   Shen, R.; Crean, R. M.; Olsen, K. J.; Corbella, M.; Calixto, A. R.; Richan, T.; Brandão, T. A. S.; Berry, R. D.; Tolman, A.; Loria, J. P.; Johnson, S. J.; Kamerlin, S. C. L.; Hengge, A. C. Insights into the Importance of WPD-Loop Sequence for Activity and Structure in Protein Tyrosine Phosphatases. *Chem. Sci.* **2022**, *13* (45), 13524–13540. https://doi.org/10.1039/D2SC04135A.

(31)   Moise, Gwendolyn; Morales, Y.; Beaumont, V.; Caradonna, T.; Loria, J. P.; Johnson, S. J.; Hengge, A. C. A YopH PTP1B Chimera Shows the Importance of the WPD-Loop Sequence to the Activity, Structure, and Dynamics of Protein Tyrosine Phosphatases. *Biochemistry* **2018**, *57* (36), 5315–5326. https://doi.org/10.1021/acs.biochem.8b00663.

(32)   Chou, P. Y.; Fasman, G. D. β-Turns in Proteins. *J. Mol. Biol.* **1977**, *115* (2), 135–175. https://doi.org/10.1016/0022-2836(77)90094-8.

(33)   Zinovjev, K.; Tuñón, I. Adaptive Finite Temperature String Method in Collective Variables. *J. Phys. Chem. A* **2017**, *121* (51), 9764–9772. https://doi.org/10.1021/acs.jpca.7b10842.

(34)   Daldrop, J. O.; Kappler, J.; Brünig, F. N.; Netz, R. R. Butane Dihedral Angle Dynamics in Water Is Dominated by Internal Friction. *Proc. Natl. Acad. Sci.* **2018**, *115* (20), 5169–5174. https://doi.org/10.1073/pnas.1722327115.

(35)   Echeverria, I.; Makarov, D. E.; Papoian, G. A. Concerted Dihedral Rotations Give Rise to Internal Friction in Unfolded Proteins. *J. Am. Chem. Soc.* **2014**, *136* (24), 8708–8713. https://doi.org/10.1021/ja503069k.

(36)   Baron Peters. *Reaction Rate Theory and Rare Events*; Elsevier, 2017.

(37)   Kramers, H. A. Brownian Motion in a Field of Force and the Diffusion Model of Chemical Reactions. *Physica* **1940**, *7* (4), 284–304. https://doi.org/10.1016/S0031-8914(40)90098-2.

(38)   Zheng, W.; de Sancho, D.; Best, R. B. Modulation of Folding Internal Friction by Local and Global Barrier Heights. *J. Phys. Chem. Lett.* **2016**, *7* (6), 1028–1034. https://doi.org/10.1021/acs.jpclett.6b00329.

(39)   Grote, R. F.; Hynes, J. T. The Stable States Picture of Chemical Reactions. II. Rate Constants for Condensed and Gas Phase Reaction Models. *J. Chem. Phys.* **1980**, *73* (6), 2715–2732. https://doi.org/10.1063/1.440485.

(40)   Das, D.; Arora, L.; Mukhopadhyay, S. Short-Range Backbone Dihedral Rotations Modulate Internal Friction in Intrinsically Disordered Proteins. *J. Am. Chem. Soc.* **2022**, *144* (4), 1739–1747. https://doi.org/10.1021/jacs.1c11236.

(41)   Gertner, B. J.; Wilson, K. R.; Hynes, J. T. Nonequilibrium Solvation Effects on Reaction Rates for Model SN2 Reactions in Water. *J. Chem. Phys.* **1989**, *90* (7), 3537–3558. https://doi.org/10.1063/1.455864.

(42)   Sawaya, M. R.; Kraut, J. Loop and Subdomain Movements in the Mechanism of Escherichia Coli Dihydrofolate Reductase: Crystallographic Evidence,. *Biochemistry* **1997**, *36* (3), 586–603. https://doi.org/10.1021/bi962337c.

(43)   Lolis, E.; Alber, T.; Davenport, R. C.; Rose, D.; Hartman, F. C.; Petsko, G. A. Structure of Yeast Triosephosphate Isomerase at 1.9-.ANG. Resolution. *Biochemistry* **1990**, *29* (28), 6609–6618. https://doi.org/10.1021/bi00480a009.

(44)   Jogl, G.; Rozovsky, S.; McDermott, A. E.; Tong, L. Optimal Alignment for Enzymatic Proton Transfer: Structure of the Michaelis Complex of Triosephosphate Isomerase at 1.2-

Å Resolution. *Proc. Natl. Acad. Sci.* **2003**, *100* (1), 50–55.
https://doi.org/10.1073/pnas.0233793100.

(45)   Świderek, K.; Panczakiewicz, A.; Bujacz, A.; Bujacz, G.; Paneth, P. Modeling of
Isotope Effects on Binding Oxamate to Lactic Dehydrogenase. *J. Phys. Chem. B* **2009**, *113*
(38), 12782–12789. https://doi.org/10.1021/jp903579x.

(46)   Ge, M.; Molt, R. W. Jr.; Jenkins, H. T.; Blackburn, G. M.; Jin, Y.; Antson, A. A.
Octahedral Trifluoromagnesate, an Anomalous Metal Fluoride Species, Stabilizes the
Transition State in a Biological Motor. *ACS Catal.* **2021**, *11* (5), 2769–2773.
https://doi.org/10.1021/acscatal.0c04500.

(47)   Kerns, S. J.; Agafonov, R. V.; Cho, Y.-J.; Pontiggia, F.; Otten, R.; Pachov, D. V.; Kutter,
S.; Phung, L. A.; Murphy, P. N.; Thai, V.; Alber, T.; Hagan, M. F.; Kern, D. The Energy
Landscape of Adenylate Kinase during Catalysis. *Nat. Struct. Mol. Biol.* **2015**, *22* (2), 124–
131. https://doi.org/10.1038/nsmb.2941.

(48)   The PyMOL Molecular Graphics System, Version 1.2r3pre, Schrödinger, LLC.

(49)   Olsson, M. H. M.; Søndergaard, C. R.; Rostkowski, M.; Jensen, J. H. PROPKA3:
Consistent Treatment of Internal and Surface Residues in Empirical PKa Predictions. *J.
Chem. Theory Comput.* **2011**, *7* (2), 525–537. https://doi.org/10.1021/ct100578z.

(50)   Tian, C.; Kasavajhala, K.; Belfon, K. A. A.; Raguette, L.; Huang, H.; Migues, A. N.;
Bickel, J.; Wang, Y.; Pincay, J.; Wu, Q.; Simmerling, C. Ff19SB: Amino-Acid-Specific Protein
Backbone Parameters Trained against Quantum Mechanics Energy Surfaces in Solution. *J.
Chem. Theory Comput.* **2020**, *16* (1), 528–552. https://doi.org/10.1021/acs.jctc.9b00591.

(51)   Izadi, S.; Anandakrishnan, R.; Onufriev, A. V. Building Water Models: A Different
Approach. *J. Phys. Chem. Lett.* **2014**, *5* (21), 3863–3871.
https://doi.org/10.1021/jz501780a.

(52)   Case, D. A.; Belfon, K.; Ben-Shalom, I. Y.; Brozell, S. R.; Cerutti, D. S.; III, T. E. C.;
Cruzeiro, V. W. D.; Darden, T. A.; Duke, R. E.; Giambasu, G.; Gilson, M. K.; Gohlke, H.;
Goetz, A. W.; Harris, R.; Izadi, S.; Izmailov, S. A.; Kasavajhala, K.; Kovalenko, A.; Krasny, R.;
Kurtzman, T.; Lee, T. S.; LeGrand, S.; Li, P.; Lin, C.; Liu, J.; Luchko, T.; Luo, R.; Man, V.; Merz,
K. M.; Miao, Y.; Mikhailovskii, O.; Monard, G.; Nguyen, H.; Onufriev, A.; Pan, F.; Pantano,
S.; Qi, R.; Roe, D. R.; Roitberg, A.; Sagui, C.; Schott-Verdugo, S.; Shen, J.; Simmerling, C. L.;
Skrynnikov, N. R.; Smith, J.; Swails, J.; Walker, R. C.; Wang, J.; Wilson, L.; Wolf, R. M.; Wu,
X.; Xiong, Y.; Xue, Y.; York, D. M.; Kollman, P. A. AMBER 2020, 2020.

(53)   Ryckaert, J.-P.; Ciccotti, G.; Berendsen, H. J. C. Numerical Integration of the
Cartesian Equations of Motion of a System with Constraints: Molecular Dynamics of n-
Alkanes. *J. Comput. Phys.* **1977**, *23* (3), 327–341. https://doi.org/10.1016/0021-
9991(77)90098-5.

(54)   Darden, T.; York, D.; Pedersen, L. Particle Mesh Ewald: An N·log(N) Method for
Ewald Sums in Large Systems. *J. Chem. Phys.* **1993**, *98* (12), 10089–10092.
https://doi.org/10.1063/1.464397.